Controlling morphology and charge transfer in ZnO/polythiophene photovoltaic films

Oded Nahor,[1] Tamar Segal-Peretz,[1] Lior Neeman,[2] Dan Oron,[2] and Gitti L. Frey[1]*

[1] Department of Materials Science & Engineering, Technion - Israel Institute of Technology, Haifa 32000, Israel

[2] Department of Physics of Complex Systems, Weizmann Institute of Science, Rehovot 76000, Israel

ABSTRACT

The organic-inorganic interfacial chemical composition and interaction have a critical influence on the performance of corresponding hybrid photovoltaic devices. Such interfaces have been shown to be controlled by using surfactants to promote contact between the organic electron-donating conjugated polymer species and the inorganic electron-accepting metal oxides. However, the location of the surfactant at the organic/inorganic interface often hinders donor/acceptor charge transfer and limits the device performance. In this study we have replaced the conventional surfactant with an optically and electronically active amphiphilic polythiophene that both compatibilizes the conjugated polymer and metal oxide, and plays an active role in the charge generation process. Specifically, a polythiophene with hydrophilic urethane side-groups allows the formation of a fine continuous ZnO network in P3HT with organic/inorganic interfacial chemical interaction and high surface area. A combination of FTIR, absorption and photoluminescence life-time spectroscopy yields insights on the composition and nano-scale interaction of the components, while high-resolution electron microscopy reveals the

morphology of the films. The control over morphology and electronic coupling at the hybrid interface is manifested in photovoltaic devices with improved performances.

1. Introduction

Organic photovoltaic devices (OPV) are promising alternative energy sources offering the combination of low cost solution processing, high optical absorption in the visible spectrum and the versatility and tunability of organic chemistry. Among the suggested OPV structures, the donor/acceptor bulk-heterojunction (BHJ) has gained most interest because the high interfacial area and continuous pathways allow efficient charge generation and transport to the respective electrodes. Accordingly, the device performance critically depends on the donor/acceptor interfacial interactions and the film morphology [1-4]. The most efficient BHJ systems currently reported utilizes a conjugated polymer donor and fullerene-derivative acceptor [5, 6]. Although this pair is simply processed from solution, the nano-scale morphology is highly sensitive to processing conditions and directing desired nanostructures is challenging [6-13]. Hybrid organic/inorganic photovoltaics (HOPVs), composed of a conjugated polymer donor and inorganic acceptor, are an alternative to OPVs offering higher control of morphology, enhanced electron conductivity and improved stability.

Hybrid OPV films require the formation of nano-scale continuous networks of the inorganic acceptor embedded in the donor polymer matrix. Of the inorganic semiconductors, metal oxides are commonly used as acceptors in hybrid OPV, mainly TiO_2 [14, 15] and ZnO [16-18]. Accordingly, several methods have been developed to prepare BHJ metal oxide/conjugated polymer photovoltaic films. In the first method, the polymer solution is spun onto a substrate with pre-formed metal oxide nanoparticles or nanotubes [19-21]. However, the incompatibility of the polymer solution and metal oxide structures limits polymer infiltration into the sub-micron sized gaps between the inorganic nanostructures.[22] Alternatively, an organometallic metal oxide precursor is added to the polymer solution prior to spin coating, followed by conversion to the metal oxide after film deposition [16-18, 23]. Here too, the mismatch between the chemical nature of the *in-situ* formed metal oxide particles and the surrounding conjugated polymer matrix could lead to a local phase separation[24]. The lack of intimate organic/inorganic interface in both

methods described above is translated to weak donor/acceptor coupling and significantly limits the device performance.

The incompatibility between conjugated polymers and metal oxides can be overcome using surfactants. The amphiphilic character of the surfactant allows the co-processing of the organic and inorganic phases into hybrid films. The films prepared from solutions using surfactants as compatibilizers show fine organic/inorganic phase separation morphologies and occasionally continuous single-phase networks. Under such conditions a considerable volume of the film is occupied by the surfactant which is located mainly at the organic/inorganic interface. Importantly, presence of such conventional non-optically active and electronically insulating surfactant at the donor/acceptor interface significantly hinders the electronic coupling [14, 15]. Therefore, while the conventional amphiphilic surfactants are useful for directing BHJ morphologies in hybrid films, their location at the organic/inorganic interface suppresses charge generation.

In this study we replace the conventional surfactant with an optically- and electronically-active amphiphilic conjugated polymer that both compatibilizes the conjugated polymer and metal oxide, and plays an active role in photocurrent generation. Specifically, a polythiophene polymer with hydrophilic urethane side-groups is used to compatibilize poly(3-hexylthiophene-2,5-diyl) (P3HT) and ZnO. The urethane group is intended to chemically interact with the ZnO to provide the required electronic coupling, while the polythiophene backbone is compatible with P3HT and prevents the organic/inorganic phase separation. Optical absorption measurements in the visible and infra-red regions confirm the presence of the organic/inorganic chemical interactions; and top-view and cross-section high resolution electron microscopy imaging confirm the nano-scale mixing of the organic and inorganic components. Finally, the electronic coupling and phase separation endowed by the compatibilizing polymer are reflected in the device performance showing an enhancement of both short circuit current, Jsc, and open circuit voltage, Voc, depending on the active layer processing.

2. Experimental Section

2.1. Materials

1,2-dichlorobenzene (DCB, ReagentPlus®), tetrahydrofuran (THF, anhydrous), and diethylzinc (DEZn, 15%wt in toluene) were purchased from Aldrich and used as received. The conjugated polymer: Poly(3-hexylthiophene-2,5-diyl) (P3HT, Mw=50,000 gr/mol, 95% regioregularity) was purchased from Reike Metals, Inc. U.S.A and used as-received. The conjugated polymer: poly[3-(2-ethyl-isocyanato-octadecanyl)-thiophene] (UPT, Mw=100,000-300,000 gr/mol) was purchased from American Dye Source, Inc. Canada and used as-received. An aqueous dispersion of poly(3,4-ethylendioxythiophene)-poly(styrenesulfonate), (PEDOT:PSS), was acquired from Haraeus (CLEVIOSTM P VP AL 4083) and was filtered in a 0.45μm PTFE filter before usage.

Substrates used in this study include glass and - ITO-covered glass. All substrates were cleaned thoroughly by sonication in acetone, methanol and isopropanol for 15 min each. Oxygen plasma treatment was applied for 5 min prior to spin coating a PEDOT:PSS solution at 2000 rpm for 1 min, followed by a heating treatment on a hot plate for 15 min at 100°C. The substrates were then transferred into a glove-box with N_2 atmosphere.

2.2. Synthesis and device preparation

Three stock solutions were prepared and kept in the N_2 glove box: P3HT in dichlorobenzene (14.3 mg ml^{-1}), UPT in anhydrous tetrahydrofuran (14.3 mg ml^{-1}), and diethylzinc (DEZn) in toluene and anhydrous tetrahydrofuran (0.4M, obtained by mixing 0.45 ml of 1.1M DEZn solution in toluene with 0.9 ml anhydrous tetrahydrofuran). The precursor solutions for film and device preparation were prepared by combining specific amounts of the three stock solutions. First, the two polymer solutions were combined at 45°C to obtain five polythiophene solutions, with 350 μl volume each, and P3HT:UPT volume ratio of: 350:0, 300:50, 250:100, 200:150 and 150:200 μl. Then, 150 μl of the DEZn solution was added to each of the five 350 μl polythiophenes mixture solutions. Under such conditions, all final precursor solutions contained 10 mg/ml polythiophenes mixture and 10 mg/ml ZnO (assuming full conversion of the DEZn to ZnO). Therefore, the compositions in wt% of the hybrid films prepared from these five solutions were: P3HT(50):UPT(0):ZnO(50), P3HT(43):UPT(7):ZnO(50), P3HT(36):UPT(14):ZnO(50), P3HT(29):UPT(21):ZnO(50) and P3HT(21):UPT(29):ZnO(50)

About 6 min after adding the DEZn solution to the polythiophenes mixture solutions, the polythiophene:DEZn solutions started to gel. Therefore, we have also studied the effect of solution ageing on the obtained morphology. This was done by varying the time between DEZn addition to the polymer mixture solution and the spin coating. This standing-time was 90, 210 or 330 sec. Film thicknesses, determined using cross-section high-resolution scanning electron microscopy, were found to be ~ 50 nm for short standing-time, regardless of composition. However, extended standing-times for solutions with UPT increased solution viscosity leading to thickness films up to ~ 70 nm. Selected images are shown in Figure 1S of the supplementary information section.

A list of the samples prepared and studied is provided in Table 1:

Table 1- Composition and standing-time of samples prepared and studied

Sample name	P3HT [wt%]	UPT [wt%]	ZnO [wt%]	Standing-time[sec]
P3HT(50):UPT(0):ZnO(50)	50	0	50	90
				210
				330
P3HT(43):UPT(7):ZnO(50)	43	7	50	90
				210
				330
P3HT(36):UPT(14):ZnO(50)	36	14	50	90
				210
				330
P3HT(29):UPT(21):ZnO(50)	29	21	50	90
				210
				330
P3HT(21):UPT(29):ZnO(50)	21	29	50	90
				210

				330
P3HT(0):UPT(50):ZnO(50)	0	50	50	330

Films on glass/ITO/PEDOT:PSS and glass/PEDOT:PSS substrates for device and optical measurements, respectively, were prepared in the glove box by spin coating the precursor solutions at 1500 rpm for 1 min and subsequent 1 min at 3000 rpm. The films were then transferred out of the glove-box and annealed at 100°C with 100% humidity for 12 min followed by 3 min at 100°C in ambient atmosphere for full conversion of the DEZn to ZnO. The films were then transferred back to the glove box to complete device fabrication. The top contact was evaporated by thermal evaporation of a 90 nm-thick Al layer and 10 nm-thick Au layer. Device fabrication was completed by post-evaporation annealing for 3 min at 90°C in an N_2 atmosphere. 14 devices of each composition were prepared and tested.

2.3. Characterization

For Fast Fourier Transform Infra-Red (FTIR) characterization powder samples (and not thin films) were prepared by drying the solutions on a polytetrafluoroethylene (PTFE) plate in room atmosphere followed by annealing at 100°C with 100% humidity for 12 min followed by 3 min at 100°C in ambient atmosphere. The dried powders were ground and pressed with KBr to form suitable pellets. The FTIR spectroscopy was carried out using a Bruker Equinox 55 in the 4000-400 cm^{-1} range. Scanner velocity was 5 KHz with 4 cm^{-1} resolution. Quantitative analysis of the FTIR spectrum was carried using OPUS 6.5 software.

The absorption spectra were measured using a Varian Cary 100 Scan UV-Vis spectrophotometer in the 350-700 nm range.

For photoluminescence (PL) decay measurements the samples were excited using a tunable pulsed laser (Coherent Chameleon Ultra II), passing through an OPO (Coherent) and a harmonic generator (Coherent), to produce 100 fs pulses at 500 nm at a repetition rate of 80 MHz, the signals were collected in intervals of 13 nm and integrated for 1 min. The laser was focused on the sample, while PL was collected using an optical fiber, and detected using a

single-photon counting avalanche photodiode (ID quantique ultralow noise id-100) with IRF of 120 ps, connected to a time-correlated single photon counter (Picoquant Hydraharp 400) for transient emission measurements. To make sure no laser light was scattered into the detector a long-pass filter (Semrock 532LP Edgebasic) together with a color glass filter (CVI cg-og-530) were used.

Device current-density–voltage (J–V) curves were measured under 100 mW/cm^2 AM 1.5G illumination (Newport Inc. 67005 solar simulator, lamp power-150W) using a Keithley 2400 source meter.

High-resolution scanning electron microscopy (HRSEM) micrographs were acquired using a Zeiss Ultra-Plus FEG-SEM operating at 1.5 KeV.

High-resolution transmission electron microscopy (HRTEM) micrographs were acquired using a FEI Titan 80-300 KeV FEG-S/TEM operating at 200 KeV. Cross section samples for HRTEM examination were done using a Focused Ion Beam integrated in the Strata 400 STEM Dual Beam system of a Field-Emission Scanning Electron Microscope (FE-SEM).

3. Results and discussion

In this study an amphiphilic conjugated polymer is used to compatibilize P3HT and ZnO, control the hybrid film morphology and direct the organic/inorganic donor/acceptor electronic coupling desired for photovoltaic performance. More specifically, an amphiphilic polythiophene allows the collective processing of P3HT and ZnO into nano-scale BHJ morphology with photocurrent generation at the organic/inorganic interface. P3HT is commonly used as a donor in hybrid and OPVs due to its broad absorption in the visible region and semi-crystalline structure which offers good carrier mobility [25, 26]. ZnO, an acceptor with respect to P3HT, [27, 28] is solution processed into crystalline particles and hence provides improved carrier mobility compared to amorphous metal oxides [23]. The conversion of diethylzinc (DEZn) to ZnO follows a sol gel process, with the hydrolysis moderated by THF, and condensation of the hydrolyzed $Zn(OH)_2$ molecules at 100 °C to form crystalline ZnO [16, 18, 29]. *In-situ* conversion of DEZn to the ZnO in the P3HT matrix could lead to a local phase separation that would limit charge separation. To compatibilize P3HT and ZnO we selected an amphiphilic polythiophene: poly[3-(2-ethyl-isocyanato-octadecanyl)-thiophene] (UPT), as shown in Figure 1. UPT contains urethane

functional side-groups that allow its high solubility in THF, a suitable solvent for P3HT and the DEZn processing. In addition, the distinct FTIR finger-print of the urethane group can be used for chemical and morphological characterization. Finally, the carbonyl of the urethane group could interact with the DEZn effectively suppressing phase separation and inducing the organic/inorganic electronic coupling necessary for photocurrent generation.
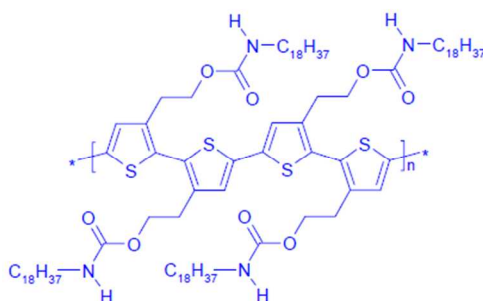

Figure 1. Chemical structure of UPT poly[3-(2-ethyl-isocyanato-octadecanyl)-thiophene].

The formation of a chemical interaction between UPT and ZnO in the hybrid materials is studied using FTIR spectroscopy. The FTIR spectra of neat UPT (red line) and a hybrid material prepared drying a 1:1 wt% mixture of the DEZn precursor solution and the UPT solution (black line) are shown in Figure 2. Comparing the two spectra in full range, Figure 2a confirms that UPT is present in the film and generally maintains its structure with the ring stretching peak of the thiophene backbone centered at 1466 cm^{-1}, the two typical urethane peaks at 1537 and 1694 cm^{-1}, and the aliphatic chain characteristic bands between 2800 to 3000 cm^{-1} [30-33]. Importantly, Figure 2a also provides first evidence for the presence of ZnO in the hybrid material showing a new band centered at 488 cm^{-1} which is associated with Zn-O stretching[33, 34]. UPT interactions with ZnO could be identified by carefully analyzing changes in the UPT spectrum when processed with ZnO (see experimental). Namely, a close look at the urethane peaks in the hybrid sample of UPT and ZnO, Figure 2b, shows an intensity decrease and broadening of both peaks in the hybrid sample compared to the neat UPT. Furthermore, integrating the area under the peaks allows quantitative analysis of the urethane:thiophen group ratio. It is found that the ratio between the urethane (1761-1491 cm^{-1}) to thiophene peak areas (1488-1400 cm^{-1}) in the neat UPT spectrum is double the value calculated for the hybrid UPT:ZnO sample. The clear broadening and intensity reduction of the urethane peaks in the FTIR spectrum of the hybrid

sample could be associated with a decrease in the number of urethane groups, possibly due to a chemical interaction with DEZn.
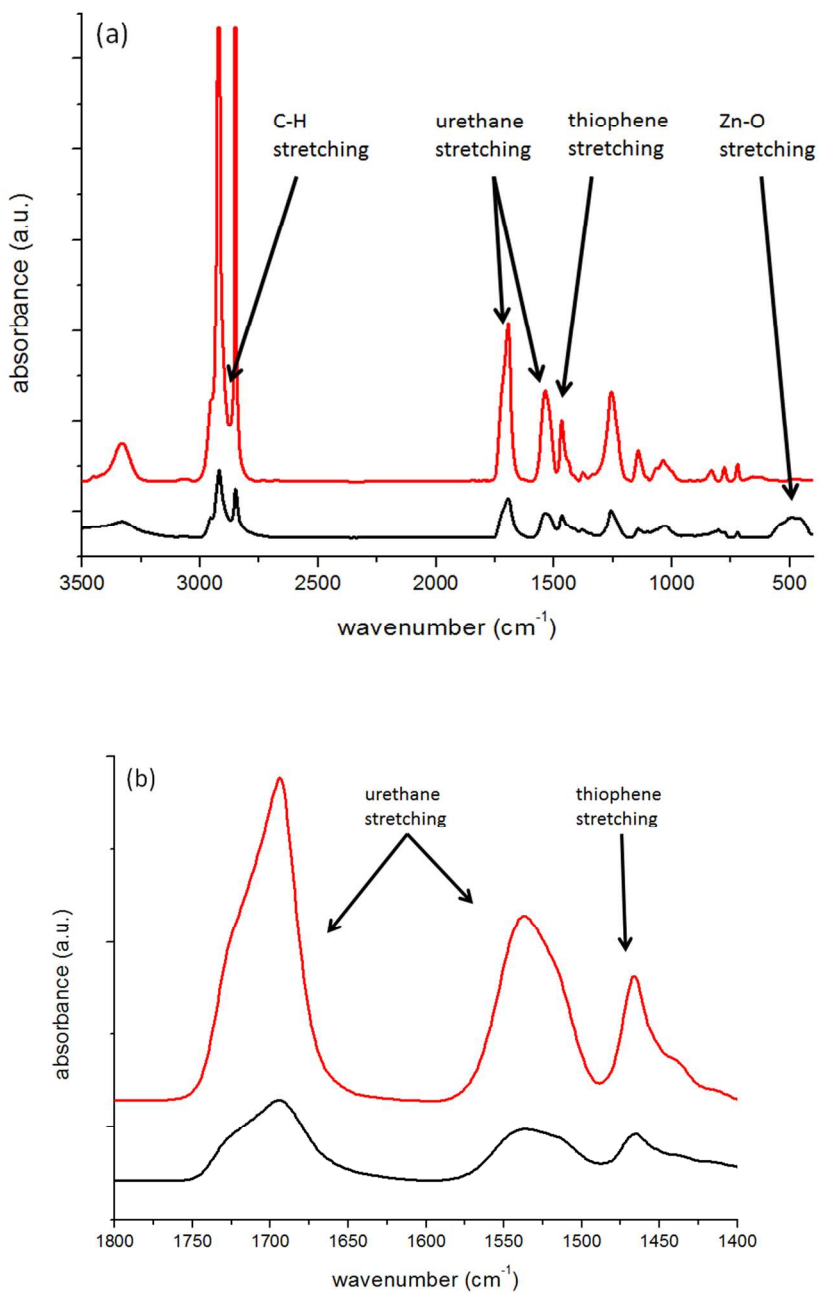

Figure 2. Full range (a), and selected range (b) FTIR spectra of neat UPT (red) and hybrid material of UPT and ZnO (black).

The effect of the chemical interaction between the UPT and ZnO on the film morphology is studied by measuring the optical absorption spectra of the hybrid films as a function of polythiophene blend composition (Figure 3a), and the standing-time prior to spinning the films (Figure 3b). The optical absorption spectrum of a neat P3HT film spun from dichlorobenzene (dashed black curve in Figure 3a) shows the typical intra-molecular vibronic transitions centered at 524 and 552 nm, and the π-π* interactions shoulder at 605 nm, indicative of highly ordered semi-crystalline domains [16, 35]. The neat UPT absorption spectrum (dashed red curve in Figure 3a), on the other hand, shows a broad featureless peak centered at 512 nm with two weak shoulders at 554 and 603 nm. The broad shape and blue shift of the UPT peaks compared to those of P3HT indicate that UPT is substantially less ordered than P3HT and probably fully amorphous. Addition of ZnO to P3HT slightly reduces P3HT ordering, as evident from the small decrease in intensity of the π-π* interactions shoulder at 605 nm in the absorption spectrum of the P3HT(50):UPT(0)ZnO(50) sample processed with no UPT (black line Figure 3a)[16]. Replacing a small amount of P3HT with UPT has little to no effect on the P3HT ordering in the film as evident from the spectrum of the P3HT(43):UPT(7):ZnO(50) sample (green line in Figure 3a). However, further increasing the amount of UPT on expense of P3HT, P3HT(36):UPT(14):ZnO(50), suppresses P3HT ordering (blue line in Figure 3a) probably due to the long aliphatic side chains of UPT disturbing thiophene chain close packing, perturbing the order and π-π* interactions in the organic phase. In addition to the blend composition, the standing-time of the hybrid solutions prior to spinning also affects film morphology. Figure 3b shows the absorption spectra of hybrid films with an identical composition: P3HT(36):UPT(14):ZnO(50), but with different elapsed-times between solution preparation and spinning. Noticeably, longer standing-time results in a reduction of the π-π* interactions shoulder reflecting lower order of the P3HT domains. This result is somewhat surprising because generally, stalling P3HT solutions prior to spinning enhances intermolecular interactions which increases the intensity of the π-π* interactions shoulder [11, 13]. We assign the suppressed P3HT ordering to the UPT-ZnO interaction which was identified in the FTIR spectra. The interaction between the UPT and DEZn is more dominant as the standing-time increases, as evident from the gelling of the solution. This chemical interaction is retained upon DEZn conversion to ZnO, evident from the FTIR spectra in Figure 2, serving as an anchor between the conjugated polymer

and the inorganic particles in the hybrid film. In parallel, the chemical resemblance between the two thiophene polymers, P3HT and UPT, supports their mixing as reflected in the reduced P3HT ordering with increased UPT content. Hence, under the condition used in this study, the UPT polymer acts as a "surfactant" effectively reducing the organic/inorganic phase separation while also generating intimate polythiophene/ZnO interfaces. Suppressing organic/inorganic separation while maintain an interfacial electronic coupling is expected to enhance exciton dissociation and charge generation in photovoltaic devices.

In addition to allowing an intimate organic/inorganic interface, the interaction between UPT and DEZn causes the solution to gel and hence also affects the thickness of the films. The contribution of standing-time to the optical absorption is analyzed by comparing the non-normalized spectra of the hybrid films. Indeed, Figure 3c shows that increasing the standing-time increases the optical absorption, as evident from comparing the spectra of P3HT(36):UPT(14):ZnO(50) with different elapsed-times (90, 210 and 330 sec). This increase is associated with an increase in film thickness due to the higher viscosity of the retained solutions with UPT. In contrast, replacing P3HT with UPT in the hybrid films causes a reduction in absorption as evident by comparing the absorption of hybrid films with the same elapsed-time, but different compositions (solid lines in Figure 3c). Figure 3c shows that the hybrid film with no UPT, P3HT(50):UPT(0):ZnO(50), has the highest absorption, which then decreases to similar values for the P3HT(43):UPT(7):ZnO(50) and P3HT(36):UPT(14):ZnO(50) films. We associate the inconsistency between the measured absorbance and film thickness that is driven by the solution viscosity, to light scattering by the ZnO nanoparticle network formed at the surface of films with UPT. Indeed, film morphology analysis (*Vida infra*) confirms that the UPT and DEZn interactions induce the formation of a ZnO nanoparticle network at the surface and through the film.
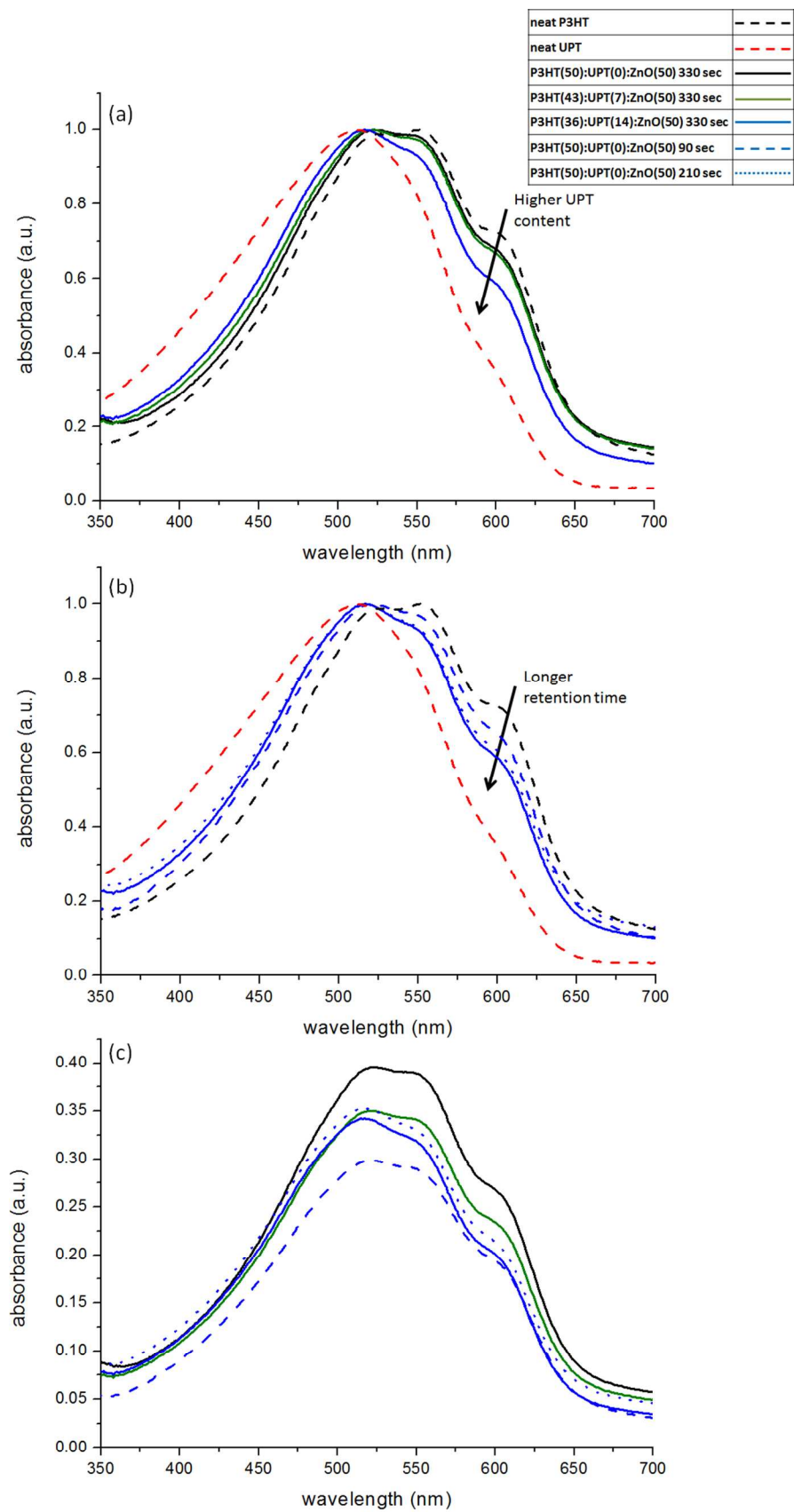
Figure 3. Normalized (a and b) and non-normalized (c) UV-vis absorption spectra of neat polymer and hybrid films. (a) as a function of polythiophene blend composition: neat P3HT film (dashed black line); neat UPT film (dashed red line); P3HT(50):UPT(0):ZnO(50) (solid black line), P3HT(43):UPT(7):ZnO(50) (solid green line) and P3HT(36):UPT(14):ZnO(50) (solid blue line) – all hybrid film were prepared with 330 sec standing-time. (b) as a function of solution standing-time of the hybrid P3HT(36):UPT(14):ZnO(50) film, prior to spinning: 90 sec (dashed blue line), 210 sec (dotted blue line) and 330 sec (solid blue line) and neat P3HT film (dashed black line); neat UPT film (dashed red line). (c) as-measured UV-vis absorption spectra of: P3HT(50):UPT(0):ZnO(50) (solid black line), P3HT(43):UPT(7):ZnO(50) (solid green line) and P3HT(36):UPT(14):ZnO(50) with different standing-times: 90 sec (dashed blue line), 210 sec (dotted blue line) and 330 sec (solid blue line).

The contribution of the organic/inorganic phase separation and interfacial interactions to the dynamics of the photo-excited state are studied using photoluminescence (PL) life-time (LT) spectroscopy measurements. More specifically, the life-time of the excited state is directly correlated with exciton dissociation and charge generation because efficient exciton dissociation and charge transfer reduces the exciton PL LT. Indeed, it has been shown that addition of ZnO to P3HT results in a decrease of PL LT due to photo-excited electron transfer from P3HT to ZnO [16, 36]. In this study the role of UPT as a surfactant and electronic mediator between ZnO and P3HT is studied by comparing the PL LT in neat polymer and hybrid films. Owing to multiple PL decay orders in polythiophenes[37-39] the weighted average life time was calculated using equation 1[40]:

$$\text{Equation 1:} \qquad I(t) = \sum_{i=1}^{3} \alpha_i \exp\left(\frac{-t}{\tau_i}\right) \;\; \Rightarrow \;\; \tau_{AV} = \frac{\displaystyle\sum_{i=1}^{3} \alpha_i \tau_i}{\displaystyle\sum_{i=1}^{3} \alpha_i}$$

Where α_i is the fraction of excited states decaying in the i-th process, τ_i is the lifetime of the i-th process and τ_{AV} is the total average lifetime.

The PL decay spectra and calculated average exciton life-time, τ_{AV}, are shown in Figure 4 and Table 2, respectively. The neat P3HT film exhibits average exciton LT of 0.5 ns (black squares in Figure 4), in good agreement with earlier reports [41]. The neat UPT (red triangles in Figure 4) exhibits a nearly double value, 0.9 ns. The long LT of the neat UPT can be related to the disordered chain structure and the lower amount of the π-π* interaction comparing to the neat P3HT [42]. Blending the two polymers (blue circles in Figure 4) results in a LT which is similar to

that of neat P3HT. This similarity could indicate charge transfer between the two polymers analogous to that observe at the interface between ordered and disordered P3HT domains [43]. Importantly, the LT measurements in Figure 4 show that the exciton life-times of all hybrid films (solid lines in Figure 4) are shorter comparing to those of the corresponding polymer films (symbol lines in Figure 4). This reduction is associated with exciton dissociation at the organic/inorganic interface and is more significant in the case of P3HT(50):UPT(0):ZnO(50), with LT shortened to 0.3 ns, compared to P3HT(0):UPT(50):ZnO(50) with LT of 0.7 ns. The somewhat moderate LT reduction in the P3HT(36):UPT(14):ZnO(50) hybrid film, to 0.4 ns only, confirms that in this case the organic/inorganic interface is rich with UPT on expense of P3HT. Although presence of the UPT at the hybrid interface seems to suppress charge transfer, it plays a crucial role in directing the hybrid film morphology, as will be discussed below.
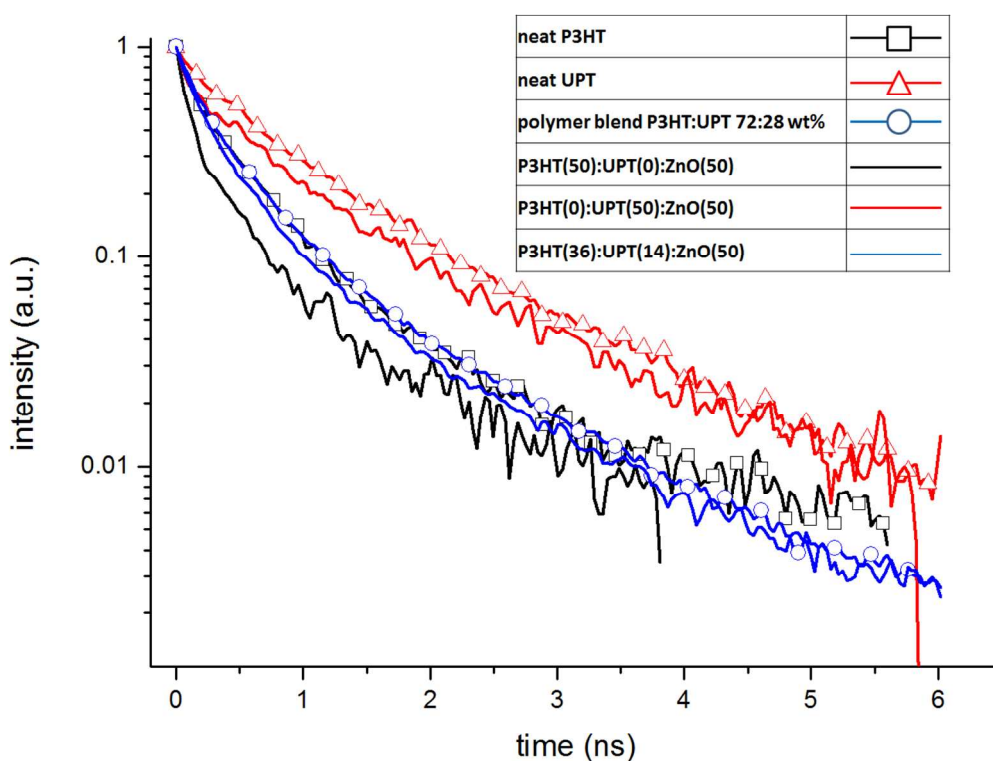

Figure 4. Normalized photoluminescence decay spectra of neat polymers, polymer blend and hybrid films: neat P3HT (black squares), neat UPT (red triangles), polymer blend P3HT:UPT 72:28 wt% (blue circles), P3HT(50):UPT(0):ZnO(50) (black line), P3HT(0):UPT(50):ZnO(50) (red line), and P3HT(36):UPT(14):ZnO(50) (blue line). All hybrid samples were prepared with 330 sec rentetion time. Experimental error is <0.05 ns for all measurements.

Table 2. Life-time summary.

sample	τ_{AV} [ns]
neat P3HT	0.5
P3HT(50):UPT(0):ZnO(50)	0.3
neat UPT	0.9
P3HT(0)UPT(50):ZnO(50)	0.7
P3HT:UPT blend (72:28)	0.5
P3HT(36):UPT(14):ZnO(50)	0.4

The morphology of the hybrid films with respect to the film composition, i.e. UPT content, and standing-time during processing is analyzed through top-view and cross-section scanning and transmission electron microscopy. A matrix of SEM micrographs showing top view images of hybrid films with increasing UPT content (x-axis) and increasing standing-time (negative y-axis) is shown in Figure 5. The bright contrast in all images represents the ZnO phase and the dark contrast represents the organic phase. For the P3HT:ZnO film with no UPT, P3HT(50):UPT(0):ZnO(50), first column in Figure 5, the images are similar and independent of standing-time showing nano-sized ZnO nanoparticles suspended in the polymer matrix. In contrast, all hybrid films with UPT show the presence of a continuous ZnO network on the surface with fine organic/inorganic phase separation. The matrix clearly shows that increasing UPT content on expense of P3HT in all hybrid films (along each row in Figure 5) results in a finer organic/inorganic phase separation. Furthermore, the standing-time also has a dramatic effect on the surface morphology as could be seen by looking down each column (identical composition, but longer elapsed-time). Generally, at short elapsed-times (first row) the surface is almost entirely coated with ZnO, while at longer elapsed-times the surface is richer with the organic phase. Since the composition is maintained along each column, the reduction of ZnO at the surface implies that increasing standing-time enhances the suspension of the inorganic phase in the bulk of the polymer film. Hence, the amount of the UPT in the blend and the standing-time provide a handle to tune the organic/inorganic phase separation in a polythiophene/ZnO hybrid film.
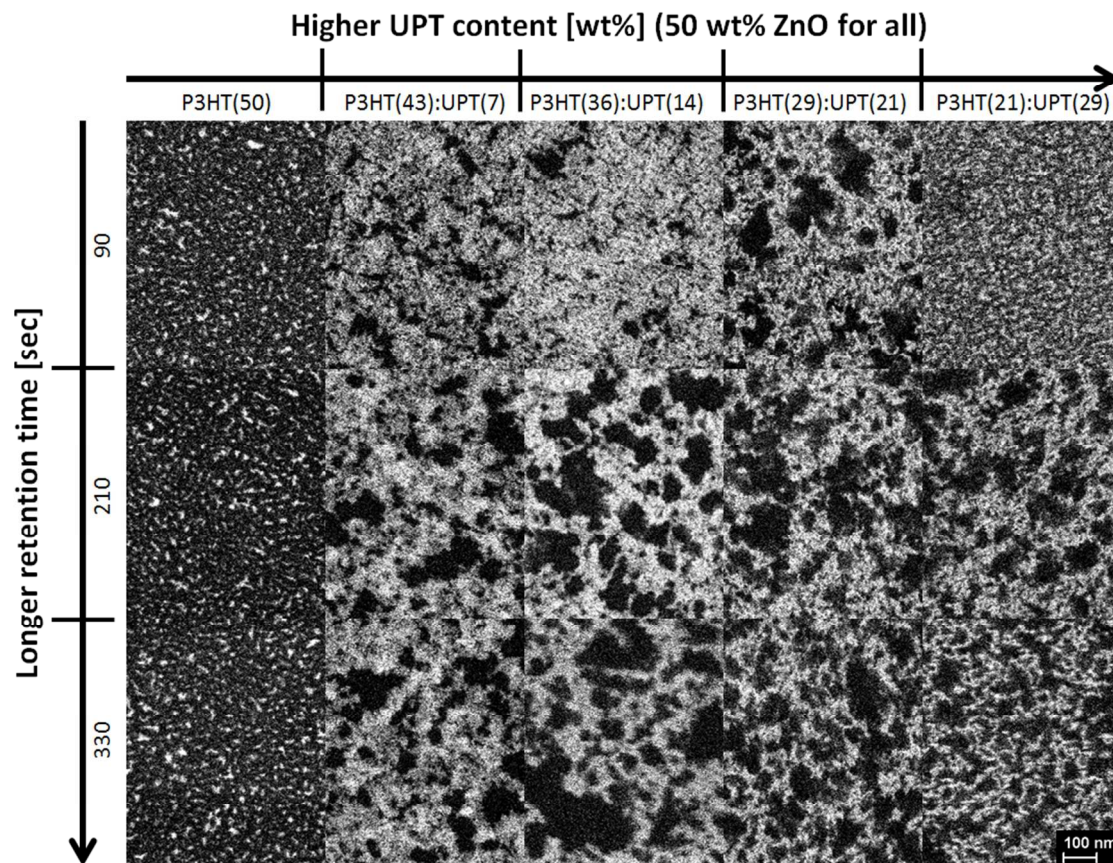
Figure 5. Matrix of top view HRSEM images of all hybrid film used in this study. The UPT content increases from left to right and standing-time increases from top to bottom.

Following the HRSEM analysis, which characterizes the surface morphology composition analysis, the 3D morphology and through-film distribution of components in the hybrid films is examined using cross-section HRTEM. Bright field micrographs of cross sections of hybrid films with different UPT content and elapsed-times are presented in Figure 6. The micrographs clearly show the active hybrid layer sandwiched between ITO and a top-evaporated Pt film (evaporated in the FIB). In the active layer, the bright contrast represents the low electron density organic phase while the dark contrast represents the higher electron density ZnO phase. The micrographs confirm the presence of ZnO particles in all hybrid films. However, in the film processed with no UPT, Figure 6a and b, the ZnO particles are clustered and located only near the top film surface (adjacent to the Pt). The high density of ZnO near the surface is in good agreement with the HRSEM surface analysis of the same film showing high density of ZnO particles at the film surface (Figure 5, first column). Partially replacing P3HT with UPT, Figure 6 c-f, results in the suspension of fine ZnO particles in the organic matrix. Initially, the ZnO

particles are still present closer to the film surface (Figure 6c and d). At even higher magnification, Figure 7, the lattice structure of an isolated ZnO particle can be identified confirming the conversion of DEZn into crystalline ZnO in the polymer matrix. Longer elapsed-times, Figure 6e and f, allow suspension of the ZnO particles through the entire polymer matrix. This deeper penetration of the ZnO particles into the bulk film is in good agreement with the HRSEM results of the same film (Figure 5, 3rd column), showing a noticeable reduction in presence of ZnO at the film surface. There, the combination of HRSEM and HRTEM results confirm that the UPT acts as a mediator to allow mixing of organic and inorganic phases into a hybrid film. Furthermore, control of the polymer blend composition and standing-time prior to spin coating can be used to direct the deposition of a hybrid film with a continuous ZnO network running through the polythiophene matrix. Therefore, judicious selection of materials and conditions allowed the deposition of hybrid films with sub-20-nm organic/inorganic phase separation and continuity of both phases through active layer is, as desired for photovoltaic
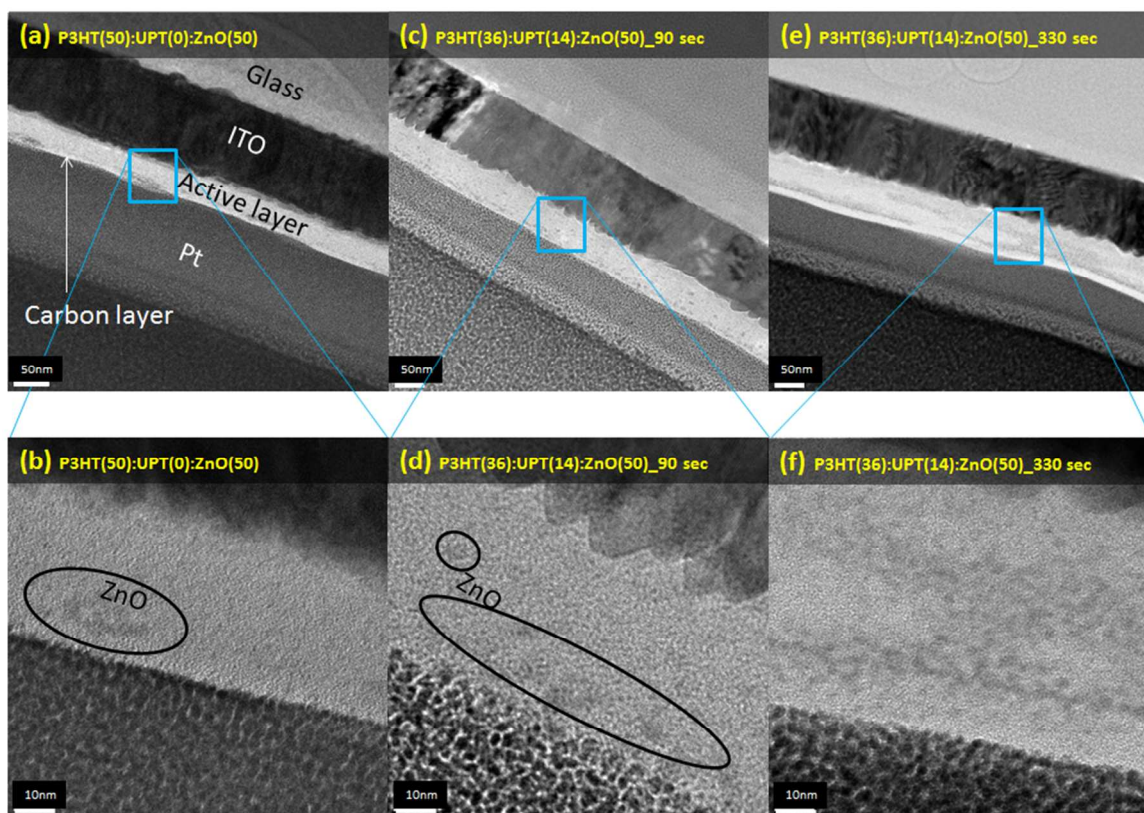

Figure 6. HRTEM micrographs of cross sections of hybrid films at low (top row) and high (bottom row) magnifications: (a,b) P3HT(50):UPT(0)ZnO(50); (c,d) P3HT(43):UPT(7)ZnO(50) prepared after 90 sec elapsed-time; (e,f) same as (c,d) but prepared after 330 sec elapsed-time.
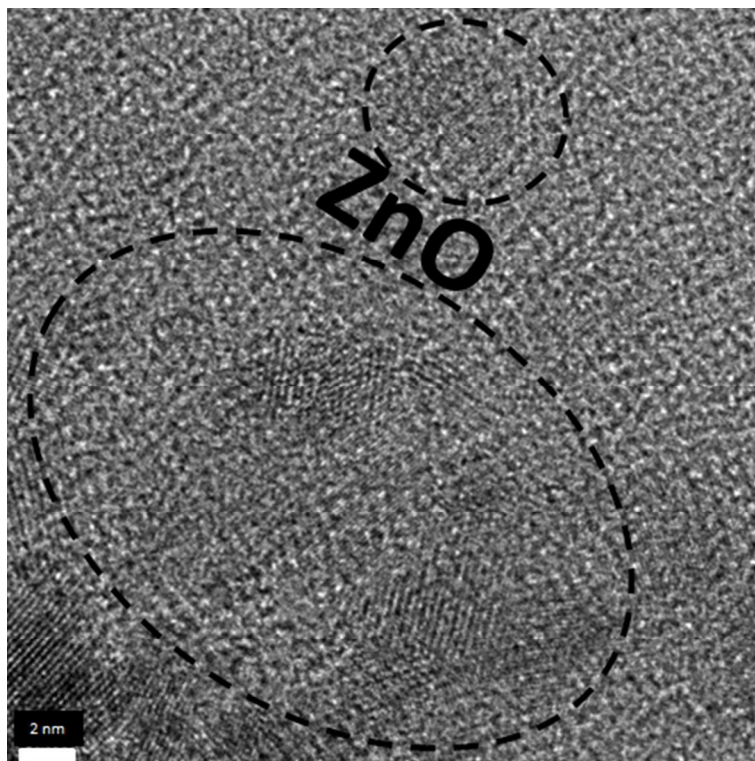
Figure 7. High magnification HRTEM micrograph of a cross section of the P3HT(36):UPT(14):ZnO(50) hybrid film with standing-time of 90 sec (same sample as Figure 6c and d).

Finally, the control over the hybrid film composition and morphology is demonstrated in photovoltaic devices. As discussed earlier, in hybrid organic/inorganic PVs the photovoltaic performance is strongly dependent on the organic/inorganic intimate interface and the nano-morphology. Thus, we anticipate that as the UPT creates intimate interface with the ZnO nanoparticles, and a continuous ZnO network is formed, the device performance will be enhanced. Accordingly, PV devices were fabricated with hybrid films processed after different elapsed-times, Figure 8a, and with different the UPT content, Figure 8b.

Figure 8a shows the performance of device with constant chemical composition (P3HT(36):UPT(14):ZnO(50)) and varying elapsed-times. The figure shows that varying the standing-time has only minor influence on the open circuit voltage, as expected from a constant chemical composition, with average Voc value of about 0.42V. On the other hand, the standing-time has a dramatic effect on the short circuit current; Jsc is increased as the standing-time is increased, from 0.04 $mAcm^{-2}$ to 0.09 $mAcm^{-2}$, and to 0.11 $mAcm^{-2}$ for devices with standing-time of 90, 210 and 330 sec, respectively. Moreover, the fill factor (FF) of the devices is also

increased with increasing the elapsed-time, from 0.39 to 0.40, and to 0.46 for the devices mentioned above. The increase in short circuit current and in the FF value with increasing standing-time was seen in all devices containing any UPT amount. The significant increase in photoinduced current is much more prominent than the increase in absorption with elapsed-time, as was seen in Figure 3c; therefore, the enhanced photocurrent is attributed to the fine phase separation and continuous ZnO pathway created at longer elapsed-times, as was seen in the electron microscopy characterization. This improved morphology enables increased charge generation and better transport to the electrodes, resulting in higher photocurrents.

Figure 8b shows the performance of devices with varying chemical composition, i.e. increasing UPT content, but similar elapsed-times (330 sec). When inspecting the effect of increasing UPT content in the hybrid films it can be seen that once UPT is incorporated into the film, Voc is increased from 0.3V for P3HT(50):ZnO(50) (black line, Figure 8b) to approximately 0.45V for P3HT(43):UPT(7):ZnO(50) green line, Figure 8b), and stabilizes as the UPT content further increases. In the short circuit current, devices with up to 14% UPT content (green and blue lines) show improved photocurrents compared to the reference device (P3HT(50):ZnO(50), black line), despite their lower absorption (Figure 3c). This increase in photocurrent values indicates that indeed UPT can enhance charge generation and extraction via a finer nano-morphology across the entire film with continuous pathways for both electrons and holes, while creating intimate polythiophene/ZnO interfaces. When examining all UPT-containing devices an interesting phenomenon is revealed: for low UPT content, the Jsc is increased as UPT content increases until a maximum value is reached and then the further increase of UPT reduces the Jsc. The maximum Jsc (0.11 $mAcm^{-2}$) is obtained for chemical composition of P3HT(36):UPT(14):ZnO(50). Correspondingly, the FF also exhibits an initial increase with UPT content from 0.36 to 0.46; but when UPT content is further increased above 14 wt% the FF value decreases. We attribute this behavior to the trade-off between improving the interfacial and nano-morphology by UPT, but lowering the hole transport. On one hand, as UPT content is increased in the film on the expanse of P3HT, an improved nano-morphology is obtained with electronic coupling between the organic and inorganic phases. On the other hand, UPT itself has lower hole mobility than P3HT, and it also hinders P3HT order and π-π* interactions; therefore, high content of UPT reduces the hole transport across the active layer. By controlling both standing-

time and chemical composition, an optimum can be found, as was seen in Figure 8b, and UPT's "surfactant" characteristics can be harnessed without significantly reducing hole transport.
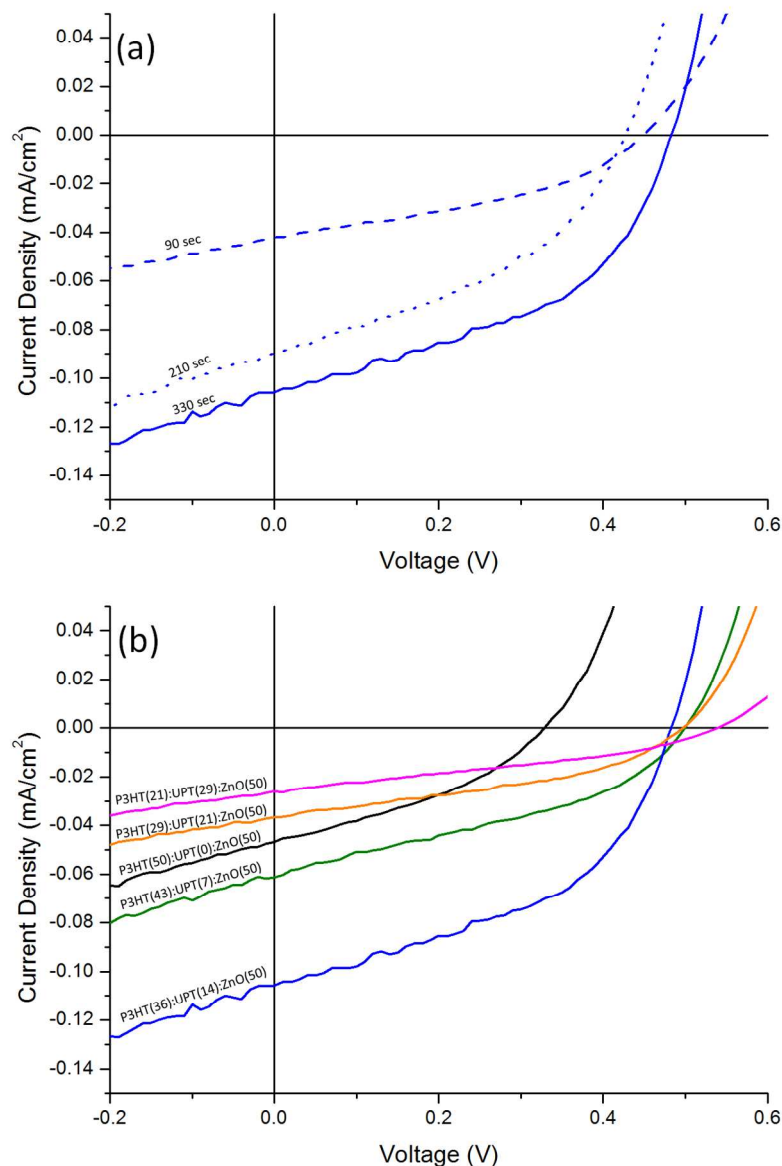

Figure 8. Photocurrent density-voltage characteristics (J-V) measured under 1.5AM illumination of PV devices with (a) different standing-time for identical composition of P3HT(36):UPT(14):ZnO(50) wt%: 90 (dashed blue), 210 (dotted blue) and 330 sec (solid blue), and with (b) different composition and constant standing-time (330 sec): P3HT(50):UPT(0):ZnO(50) (black line), P3HT(43):UPT(7):ZnO(50) (green line), P3HT(36):UPT(14):ZnO(50) (blue line), P3HT(29):UPT(21):ZnO(50) (orange line) and P3HT(21):UPT(29):ZnO(50) (magenta line). The statistics of the device performances are provided in Table 1S of the *supplementary information* section.

4. Conclusions

In this study, the organic-inorganic interface of BHJ metal oxide-conjugated polymer solar cells was controlled by introducing UPT, an amphiphilic conjugated polymer, into P3HT/ZnO BHJ films. UPT functions as an optically and electronically active surfactant; the urethane side groups chemically interact with ZnO surface, while the polythiophene backbone assimilates with P3HT. In other words, the amphiphilic conjugated polymer mediates between P3HT and ZnO network while being an optically active component. The interaction of UPT's urethane side groups with ZnO surface creates electronic coupling between the organic conjugated polymer and the inorganic metal oxide, which enables higher photocurrent generation at organic-inorganic interface. In addition, the amphiphilic nature of UPT can be harnessed to create a desired effect on the BHJ morphology. By controlling the chemical composition of the spin casted blend and the process conditions (elapsed-time), a sub-20-nm organic/inorganic phase separation and continuity of both phases through the active layer can be directed, as evident from scanning and transmission electron microscopy. This improved morphology together with the intimate interface created between UPT and ZnO induces higher performances in photovoltaic devices based on ZnO/UPT/P3HT active layer. However, the insulating side chains on the UPT might suppress electronic transport and hence blend composition must be optimized. This research has shown that amphiphilic conjugated polymers can replace conventional non-active surfactants to compatibilize organic and inorganic components in hybrid PV films while playing an active role in photocurrent generation.

AUTHOR INFORMATION

Corresponding Author

*E-mail: gitti@tx.technion.ac.il

REFERENCES

1. K. M. Coakley and M. D. McGehee, *Chemistry of Materials*, 2004, **16**, 4533-4542.
2. S. Gunes, H. Neugebauer and N. S. Sariciftci, *Chemical Reviews*, 2007, **107**, 1324-1338.
3. H. Hoppe and N. S. Sariciftci, *J. Mater. Res.*, 2004, **19**, 1924-1945.
4. B. Kippelen and J.-L. Bredas, *Energy & Environmental Science*, 2009, **2**, 251-261.
5. L. D. Jingbi Y., Ken Y., Takehito K., Kenichiro O., Tom M., Keith E., Chun-Chao C., Jing G., Gang L., Yang Y., *Nat Commun*, 2013, **4**.
6. S. H. Park, A. Roy, S. Beaupre, S. Cho, N. Coates, J. S. Moon, D. Moses, M. Leclerc, K. Lee and A. J. Heeger, *Nature Photonics*, 2009, **3**, 297-U295.
7. H.-Y. Chen, H. Yang, G. Yang, S. Sista, R. Zadoyan, G. Li and Y. Yang, *The Journal of Physical Chemistry C*, 2009, **113**, 7946-7953.
8. J. Jo, S.-I. Na, S.-S. Kim, T.-W. Lee, Y. Chung, S.-J. Kang, D. Vak and D.-Y. Kim, *Advanced Functional Materials*, 2009, **19**, 2398-2406.
9. J. K. Lee, W. L. Ma, C. J. Brabec, J. Yuen, J. S. Moon, J. Y. Kim, K. Lee, G. C. Bazan and A. J. Heeger, *Journal of the American Chemical Society*, 2008, **130**, 3619-3623.
10. A. C. Mayer, M. F. Toney, S. R. Scully, J. Rivnay, C. J. Brabec, M. Scharber, M. Koppe, M. Heeney, I. McCulloch and M. D. McGehee, *Advanced Functional Materials*, 2009, **19**, 1173-1179.
11. V. D. Mihailetchi, H. Xie, B. de Boer, L. M. Popescu, J. C. Hummelen, P. W. M. Blom and L. J. A. Koster, *Applied Physics Letters*, 2006, **89**, 012107-012103.
12. M. C. Scharber, D. Mühlbacher, M. Koppe, P. Denk, C. Waldauf, A. J. Heeger and C. J. Brabec, *Advanced Materials*, 2006, **18**, 789-794.
13. S. E. Shaheen, C. J. Brabec, N. S. Sariciftci, F. Padinger, T. Fromherz and J. C. Hummelen, *Applied Physics Letters*, 2001, **78**, 841-843.
14. S. Neyshtadt, M. Kalina and G. L. Frey, *Advanced Materials*, 2008, **20**, 2541-2546.
15. T. Segal-Peretz, O. Leman, A. M. Nardes and G. L. Frey, *The Journal of Physical Chemistry C*, 2011, **116**, 2024-2032.
16. W. J. E. Beek, M. M. Wienk and R. A. J. Janssen, *Advanced Functional Materials*, 2006, **16**, 1112-1116.
17. W. J. E. Beek, M. M. Wienk, M. Kemerink, X. Yang and R. A. J. Janssen, *The Journal of Physical Chemistry B*, 2005, **109**, 9505-9516.
18. S. D. Oosterhout, M. M. Wienk, S. S. van Bavel, R. Thiedmann, L. Jan Anton Koster, J. Gilot, J. Loos, V. Schmidt and R. A. J. Janssen, *Nat Mater*, 2009, **8**, 818-824.
19. C. Y. Kuo, W. C. Tang, C. Gau, T. F. Guo and D. Z. Jeng, *Applied Physics Letters*, 2008, **93**, 033307-033303.
20. S. S. Williams, M. J. Hampton, V. Gowrishankar, I. K. Ding, J. L. Templeton, E. T. Samulski, J. M. DeSimone and M. D. McGehee, *Chemistry of Materials*, 2008, **20**, 5229-5234.
21. D. C. Olson, Y.-J. Lee, M. S. White, N. Kopidakis, S. E. Shaheen, D. S. Ginley, J. A. Voigt and J. W. P. Hsu, *The Journal of Physical Chemistry C*, 2007, **111**, 16640-16645.
22. G. P. Bartholomew and A. J. Heeger, *Advanced Functional Materials*, 2005, **15**, 677-682.
23. D. J. D. Moet, L. J. A. Koster, B. de Boer and P. W. M. Blom, *Chemistry of Materials*, 2007, **19**, 5856-5861.
24. S. D. Oosterhout, L. Koster, S. S. van Bavel, J. Loos, O. Stenzel, R. Thiedmann, V. Schmidt, B. Campo, T. J. Cleij and L. Lutzen, *Advanced Energy Materials*, 2011, **1**, 90-96.

25.   E. J. W. Crossland, K. Tremel, F. Fischer, K. Rahimi, G. Reiter, U. Steiner and S. Ludwigs, *Advanced Materials*, 2012, **24**, 839-844.

26.   H. Sirringhaus, P. J. Brown, R. H. Friend, M. M. Nielsen, K. Bechgaard, B. M. W. Langeveld-Voss, A. J. H. Spiering, R. A. J. Janssen, E. W. Meijer, P. Herwig and D. M. de Leeuw, *Nature*, 1999, **401**, 685-688.

27.   K. Noori and F. Giustino, *Advanced Functional Materials*, 2012, **22**, 5089-5095.

28.   E. L. Ratcliff, B. Zacher and N. R. Armstrong, *The Journal of Physical Chemistry Letters*, 2011, **2**, 1337-1350.

29.   Y. S. Kim and Y. S. Won, *Bull. Korean Chem. Soc*, 2009, **30**, 1573.

30.   Y. Du, S. Z. Shen, W. D. Yang, K. F. Cai and P. S. Casey, *Synthetic Metals*, 2012, **162**, 375-380.

31.   R. Koizhaiganova, H. J. Kim, T. Vasudevan, S. Kudaibergenov and M. S. Lee, *Journal of Applied Polymer Science*, 2010, **115**, 2448-2454.

32.   O. R. Pardini and J. I. Amalvy, *Journal of Applied Polymer Science*, 2008, **107**, 1207-1214.

33.   L. Zhang, F. Li, Y. Chen, X. Peng and W. Zhou, *Journal of Luminescence*, 2010, **130**, 2332-2338.

34.   A. E. Jiménez-González, J. A. Soto Urueta and R. Suárez-Parra, *Journal of Crystal Growth*, 1998, **192**, 430-438.

35.   P. Vanlaeke, A. Swinnen, I. Haeldermans, G. Vanhoyland, T. Aernouts, D. Cheyns, C. Deibel, J. D'Haen, P. Heremans, J. Poortmans and J. V. Manca, *Solar Energy Materials and Solar Cells*, 2006, **90**, 2150-2158.

36.   Y.-Y. Lin, Y.-Y. Lee, L. Chang, J.-J. Wu and C.-W. Chen, *Applied Physics Letters*, 2009, **94**, 063308.

37.   X. Ai, N. Anderson, J. Guo, J. Kowalik, L. M. Tolbert and T. Lian, *The Journal of Physical Chemistry B*, 2006, **110**, 25496-25503.

38.   J. Albero, E. Martinez-Ferrero, J. Ajuria, C. Waldauf, R. Pacios and E. Palomares, *Physical Chemistry Chemical Physics*, 2009, **11**, 9644-9647.

39.   M. T. Lloyd, R. P. Prasankumar, M. B. Sinclair, A. C. Mayer, D. C. Olson and J. W. P. Hsu, *Journal of Materials Chemistry*, 2009, **19**, 4609-4614.

40.   S. Buhbut, S. Itzhakov, E. Tauber, M. Shalom, I. Hod, T. Geiger, Y. Garini, D. Oron and A. Zaban, *ACS Nano*, 2010, **4**, 1293-1298.

41.   D. M. O'Carroll, C. E. Hofmann and H. A. Atwater, *Advanced Materials*, 2010, **22**, 1223-1227.

42.   S. Carlos, M. R. David, S. D. Anoop, M. H. Laura, D. Clément, C. G. Neil, C. A. Ana, S. Sepas, M. Klaus and H. F. Richard, *Journal of Physics: Condensed Matter*, 2002, **14**, 9803.

43.   O. G. Reid, J. A. N. Malik, G. Latini, S. Dayal, N. Kopidakis, C. Silva, N. Stingelin and G. Rumbles, *Journal of Polymer Science Part B: Polymer Physics*, 2012, **50**, 27-37.